Icarus 221 (2012) 1162–1172

Contents lists available at SciVerse ScienceDirect

Icarus

journal homepage: www.elsevier.com/locate/icarus

# High surface porosity as the origin of emissivity features in asteroid spectra

P. Vernazza [a,f,*], M. Delbo [b], P.L. King [c], M.R.M. Izawa [d], J. Olofsson [e], P. Lamy [f], F. Cipriani [g], R.P. Binzel [h], F. Marchis [i], B. Merín [j], A. Tamanai [k]

[a] European Southern Observatory, K. Schwarzschild-Str. 2, 85748 Garching, Germany
[b] UNS–CNRS–Observatoire de la Côte d'Azur, Laboratoire Lagrange, BP 4229, 06304 Nice Cedex 04, France
[c] Australian National University, Research School of Earth Sciences, Acton, ACT 0200, Australia
[d] Department of Earth Sciences, University of Western Ontario, London, Ontario, Canada
[e] Max Planck Institute for Astronomy, Königstuhl 17, 69117 Heidelberg, Germany
[f] Laboratoire d'Astrophysique de Marseille, UMR 7326, CNRS/Université d'Aix-Marseille, 38 rue Frédéric Joliot-Curie, 13388 Marseille Cedex 13, France
[g] Research and Scientific Support Department, European Space Agency, Keplerlaan 1, 2201 AZ Noordwijk, The Netherlands
[h] Department of Earth, Atmospheric, and Planetary Sciences, Massachusetts Institute of Technology, Cambridge, MA 02139, USA
[i] SETI Institute, 515 N. Whisman Road, Mountain View, CA 94043, USA
[j] Herschel Science Centre, SRE-SDH, ESA, PO Box 78, 28691 Villanueva de la Cañada, Madrid, Spain
[k] Kirchhoff-Institut für Physik, D-69120 Heidelberg, Germany

ARTICLE INFO

*Article history:*
Available online 19 April 2012

*Keywords:*
Asteroids
Composition
Regoliths
Infrared observations
Meteorites

ABSTRACT

Emission features in the mid-IR domain (7–25 μm) are quite ubiquitous among large asteroids and therefore offer the potential to uncover their surface composition. However, when comparing these spectra with the actual laboratory spectra of both minerals and meteorites, they do not necessarily match. Here, and in a companion paper by King et al. (in preparation, 2012), we show that by modifying the sample preparation – typically by suspending meteorite and/or mineral powder (<30 μm) in IR-transparent KBr (potassium bromide) powder – we are able to reproduce the spectral behavior of those main-belt asteroids with emissivity features. This resulting good match between KBr-diluted meteorite spectra and asteroid spectra suggests an important surface porosity (>90%) for the first millimeter for our asteroid sample. It therefore appears that mid-IR emission spectra of asteroids do not only carry information about their surface composition but they can also help us constraining their surface structure (underdense versus compact surface structure), as suggested by Emery et al. (Emery, J.P., Cruikshank, D.P., van Cleve, J. [2006]. Icarus 182, 496–512) in the case of the Jupiter Trojans. The large surface porosity inferred from the mid-IR spectra of certain asteroids is also implied by two other independent measurements, namely their thermal inertia and their radar albedo. We further clarified how much compositional information can be retrieved from the mid-IR range by focusing our analysis on a single object, 624 Hektor. We showed that the mid-IR range provides critical constraints (i) on its origin and of that of the red Trojans that we locate in the formation regions of the comets, and (ii) on the primordial composition of the dust present in the outer region (>10 AU) of the Solar System's protoplanetary disk. Future investigations should focus on finding the mechanism responsible for creating such high surface porosity.



## 1. Introduction

Today's asteroid belt may not only be populated by objects that formed in situ, typically between 2.2 and 3.3 AU, but also by bodies that formed over a very large range of radial distances. Bottke et al. (2006) proposed that a small population of planetesimals that formed in the terrestrial planet region might have been scattered in the main belt by emerging protoplanets early in its history. Later on, Levison et al. (2009) showed that the violent dynamical evolution of the giant-planet orbits required by the so-called Nice model (Gomes et al., 2005; Tsiganis et al., 2005; Morbidelli et al., 2005) led to the insertion of primitive trans-neptunian objects into the outer belt. A new dynamical scenario proposed by Walsh et al. (2011) – invoking an early inward migration of Jupiter to 1.5 AU in order to explain Mars' low mass – shows that the asteroid belt region may comprise inner-belt (~1–3 AU) as well as outer-belt (~4–13 AU) bodies. Taken together, these different studies suggest that the current asteroid belt might be a condensed version of the primordial Solar System, containing for example the long-lost precursors of Solar System planets such as the Earth. In this context, constraining the surface composition of asteroids may both provide constrains to these models and allow us to answer the following key questions: "What was the compositional gradient

* Corresponding author at: European Southern Observatory, K. Schwarzschild-Str. 2, 85748 Garching, Germany.
*E-mail addresses:* pvernazz@eso.org, pierre.vernazza@oamp.fr (P. Vernazza).

0019-1035/$ - see front matter © 2012 Elsevier Inc. All rights reserved.
http://dx.doi.org/10.1016/j.icarus.2012.04.003

in the Solar System at the time of planetary formation?", and "What was the composition of the building blocks of the telluric planets and the giant planet cores?"

Up to now, spectroscopy in the visible and near-infrared range (VNIR, 0.4–2.5 μm) has proven to be a powerful tool for constraining the surface composition of certain asteroid taxonomic classes that display prominent spectral features (e.g., A-, S- and V-classes) and has allowed researchers to determine the linkages between a few meteorite classes (HEDs, OCs) and their parent bodies (V- types, S-types), see works by McCord et al. (1970), Cruikshank and Hartmann (1984), Binzel and Xu (1993), Gaffey et al. (1993), Gaffey (1997), Lazzaro et al. (2000), Binzel et al. (2001, 2009, 2010), Duffard et al. (2004), Sunshine et al. (2004, 2007), Vernazza et al. (2005, 2008, 2009b), Roig et al. (2008), Moskovitz et al. (2008), Reddy et al. (2009, 2010, 2011), de León et al. (2010, 2012), Ziffer et al. (2011). However, for many asteroid classes that are featureless in this wavelength range (e.g., the B-, C-, and D-classes; Hiroi et al., 2001; Clark et al., 2010), VNIR spectroscopy remains ambiguous because some important minerals do not have features in this spectral region.

Spectroscopy in the mid-IR (7–25 μm) may provide additional compositional information and a link between asteroids and meteorites (Emery et al., 2006). Most major mineral groups and silicate glasses (such as the plagioclase feldspars) that lack useful diagnostic features at visible to near-IR wavelengths do exhibit diagnostic mid-IR features. However, it has recently been shown that, in the case of asteroids, even if the meteoritic analog and/or the main surface minerals are well known from the VNIR range, spectral deconvolution using existing mid-IR spectral libraries do not indicate their presence nor constrain their relative abundance (Vernazza et al., 2010). This suggests as a testable hypothesis that a process is taking place at the surface of some asteroids, that affects the regolith and that is not presently reproduced in the preparation of the laboratory samples.

Here, and in a companion paper by King et al. (in preparation, 2012, thereafter K12), we investigate whether the porosity of the surface may be an important factor controlling the measured mid-IR spectral properties of asteroids. We first demonstrate that by modifying the sample preparation – typically by suspending meteorite and/or mineral powder (<30 μm) in IR-transparent KBr (potassium bromide) powder – we are able to reproduce the spectral behavior of those main-belt asteroids with emissivity features. This resulting good match between KBr-diluted meteorite spectra and asteroid spectra implies an important surface porosity (>90%) for the first millimeter for our asteroid sample. Such important surface porosity is consistent with the one reported by Emery et al. (2006) in the case of the Jupiter Trojans. Second, we present independent evidences of the high surface porosity of large main belt asteroids coming from their thermal inertia and their radar albedo. Third, we investigate various mechanisms that may explain this high surface porosity. Finally, we try to clarify how much compositional information can be retrieved from the mid-IR range by focusing our analysis on a single object, 624 Hektor. In particular, we show that the mid-IR range provides critical constraints on its origin and of that of the red Trojans in general.

## 2. Mid-IR spectral properties of large main belt asteroids suggest a high surface porosity

In Fig. 1, we show the emissivity spectra of several large main belt asteroids over the wavelength range of 8–25 μm based on published data as well as data to be presented in a forthcoming paper by Marchis et al. (submitted for publication). A common feature to all spectra is the presence of a strong 10-μm emissivity band, irrespective of an object's taxonomic type, the latter being derived from spectroscopic measurements in the VNIR range (see Fig. 2; and DeMeo et al., 2009). Note that such 10-μm band has already been detected in the spectra of a few outer belt asteroids (Licandro et al., 2011, 2012) and in the spectra of the Jupiter Trojans (Emery et al., 2006).

To evaluate the information that can be retrieved from this 10-μm band, we searched for the presence of such an emissivity feature both in mid-IR laboratory measurements of meteorites and in the mid-IR spectra of solar and extra Solar System objects. We found that such a band is only seen in the following cases.

*Case A*: only in some carbonaceous chondrite meteorite spectra (mostly among COs and CVs) cataloged in the RELAB and ASTER databases.[1]
*Case B*: in all new mid-IR laboratory measurements of KBr-diluted meteorites obtained at the University of New Mexico (Fig. 3; see K12).
*Case C*: in the spectra of young protoplanetary disks around low-mass stars (Fig. 4), comets (e.g., Hale–Bopp observed with ISO by Crovisier et al. (1997)), some outer belt asteroids (Licandro et al., 2011, 2012) and Trojan asteroids (Emery et al., 2006).

In case A, an analysis of the position of the 10 μm band of the carbonaceous chondrite meteorites shows that CO and CV types provide the closest match (yet not satisfactory) to the asteroid spectra shown in Fig. 1. It is therefore not surprising that CO and CV meteorites have systematically been considered as the closest – and sometimes as likely – meteoritic analogs during previous investigations of asteroids displaying a 10 μm emissivity feature (Barucci et al., 2002 for 10 Hygiea; Dotto et al., 2004 for 308 Polyxo; Barucci et al., 2008 for 21 Lutetia). Since the 10 μm band in the meteorite spectra extends to longer wavelengths than in the asteroid data, and the spectral slope in the meteorite spectra is steeper near 14 μm (i.e., a narrower transparency minimum), it is quite unlikely that CO and CV meteorites would actually be the meteoritic analogs of these objects (e.g., see Fig. A6 in Vernazza et al. (2011) in the case of 21 Lutetia).

In case B, new mid-IR laboratory measurements show that all kinds of meteorite have a similar spectral behavior in the mid-IR when they are diluted in KBr (Fig. 3; see K12), namely they all display a 10 μm emissivity feature in their mid-IR spectrum. In addition, the property of the 10 μm band (position, width, intensity) varies with the meteorite-class and therefore the composition of a given sample (see K12). Overall, the spectral behavior resulting from those experiments matches closely the global trend seen among large asteroids: whatever the surface composition (we recall here that the 10-μm band is seen for different taxonomic types which are in most cases a proxy for composition), a remarkable variation of the 10-μm band profile (position, width, intensity) is observed (Fig. 3). The similarity between the KBr-diluted meteorite and the asteroid spectra suggests that the new sample preparation method (Izawa et al., 2010; King et al., 2011, K12) better reproduces the actual properties of asteroid regolith. This suggests a high level of porosity of the surface regolith for those asteroids as independently indicated by both the objects thermal inertia and radar albedo (see next section).

In case C, the similarity between the asteroid (624 Hektor) and both cometary and protoplanetary disk spectra (Fig. 4) implies not only comparable compositions but also similar scattering properties suggesting a highly porous surface in the asteroidal case as an analog to particles floating in space in the cometary and disk cases.

In conclusion, the 10 μm band observed in the asteroid spectra does therefore not only carry information about the surface

[1] http://www.planetary.brown.edu/relab/, http://speclib.jpl.nasa.gov/.

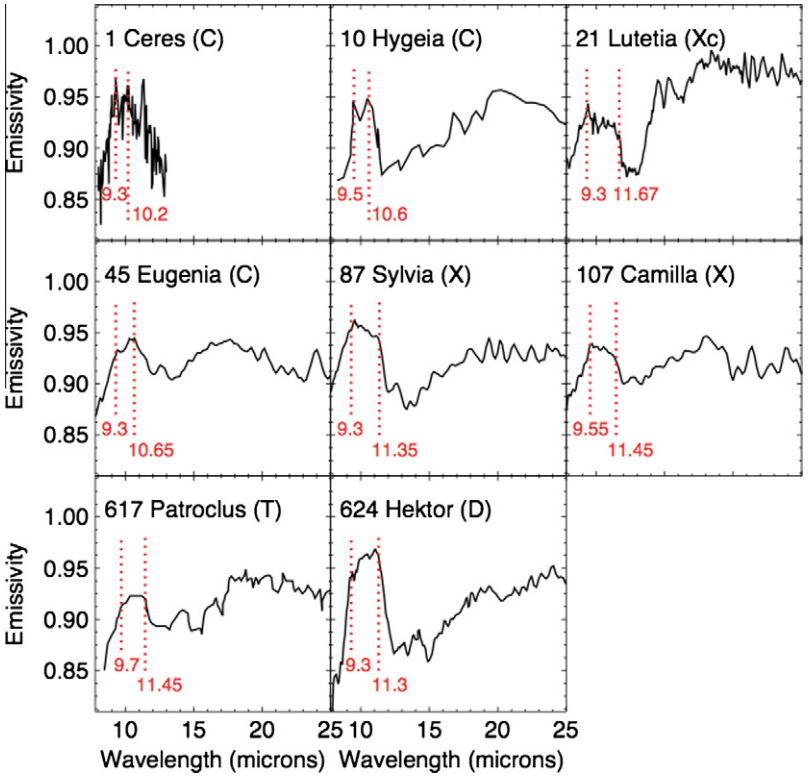


**Fig. 1.** Emissivity spectra of 1 Ceres (Cohen et al., 1998), 10 Hygeia (Barucci et al., 2002), 21 Lutetia (Barucci et al., 2008), 45 Eugenia (Marchis et al., submitted for publication), 87 Sylvia (Marchis et al., submitted for publication), 107 Camilla (Marchis et al., submitted for publication), 617 Patroclus (Mueller et al., 2010), and 624 Hektor (Emery et al., 2006). We indicate the position (start and end) of the 10-μm peak with dotted red lines. (For interpretation of the references to color in this figure legend, the reader is referred to the web version of this article.)

composition but also about the surface structural condition (prominently, compaction) of the regolith, as suggested by Emery et al. (2006) in the case of the Jupiter Trojans.

## 3. Other indicators of surface porosity

In this section, we present independent evidences of the high surface porosity of large main belt asteroids coming from their thermal inertia and their radar albedo.

### 3.1. Thermal inertia

The thermal inertia defined by $\Gamma = (\rho\kappa C)^{1/2}$ where $\rho$ is the density of the surface regolith, $\kappa$ its thermal conductivity and $C$ its heat capacity is a good indicator of the internal cohesion of the top layer (~1–10 mm). It is indeed well known that porosity affects the thermal conductivity of a material and consequently its thermal inertia (Zimbelman, 1986). For a given surface composition, the higher the porosity, the lower the values of both $\kappa$ and $\Gamma$.

For large asteroids (diameter >100 km), the value of the thermal inertia of the surface has been found to be very low (in general between ~5 and ~100 J m$^{-2}$ s$^{-0.5}$ K$^{-1}$; Delbo' et al., 2007 and references therein, Delbo' and Tanga, 2009; Mueller et al., 2010; Marchis et al., submitted for publication) compared to the typical values of meteorites as detailed below. Opeil et al. (2010) have measured the value of $\kappa$ for different meteorites encompassing nearly all known types, at temperatures ranging from 100 to 300 K. They found composition-dependent values for $\kappa$ ranging from 0.5 (carbonaceous chondrites) to 22.4 W m$^{-1}$ K$^{-1}$ (iron meteorite). Because the density of these meteorites is well known (Consolmagno et al., 2008), we could estimate the value of their thermal inertia (assuming a given value for the heat capacity) and found a range of 645–8048 J m$^{-2}$ s$^{-0.5}$ K$^{-1}$ (at 200 K). These values are at least two orders of magnitude higher than those determined for large asteroids indicating that the surface of these objects must be highly porous.

Several authors have studied the link between porosity and thermal inertia. In the case of terrestrial basalts (lavas), Zimbelman (1986) obtained a quasi-linear relation between the thermal inertia and the quantity '1 – porosity' from laboratory data acquired at atmospheric pressure. It is however well known that the heat transport of the gas plays an important role in the value of the effective conductivity of a material. Consolmagno et al. (2010) performed laboratory measurements under vacuum conditions of the heat conduction in meteorites and showed that the thermal conductivity is proportional to the inverse of the porosity of a sample.

Either way, in order to reduce the thermal inertia of a material by at least two orders of magnitude (from the lowest measured thermal inertia of a meteorite, 645 J m$^{-2}$ s$^{-0.5}$ K$^{-1}$, to the typical values for the largest asteroids, 25 J m$^{-2}$ s$^{-0.5}$ K$^{-1}$), a very large porosity (>90%) of the surface regolith is required. This is consistent with a surface layer with a very under-dense or fairy-castle-like structure (Emery et al., 2006).

### 3.2. Radar albedo

The propagation of centimeter waves in the top layer of a solid body (~1 m) is known to be critically dependent upon its composition and density.

Shepard et al. (2010) have developed a heuristic model for the radar reflectivity of asteroid surfaces covered by a regolith several meters thick, in order to estimate its density. Of interest to the present study is the fact that they were able to constrain the surface porosity by comparing their estimated surface densities

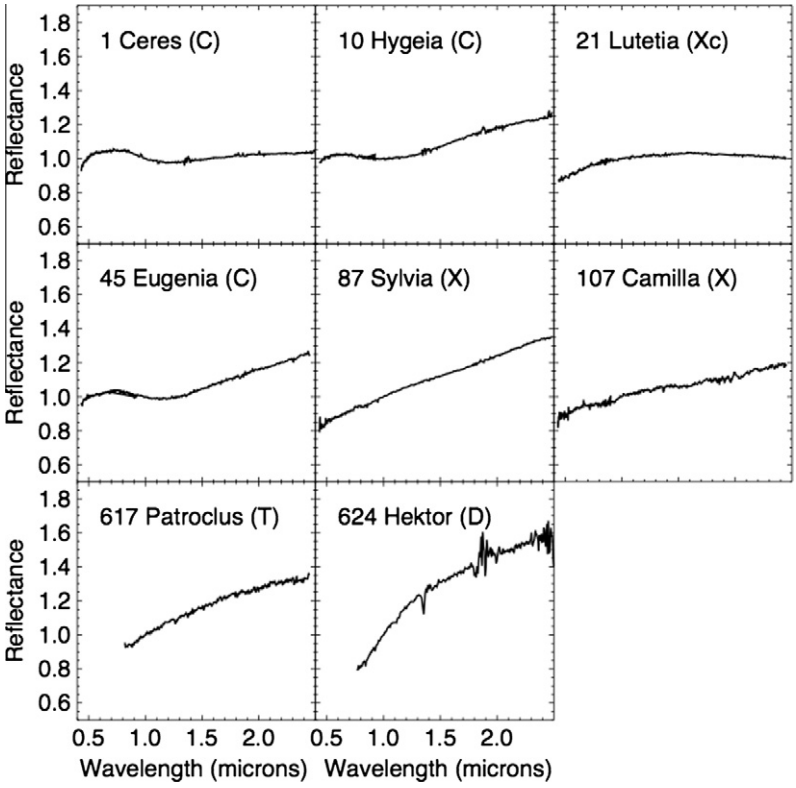


**Fig. 2.** VNIR reflectance spectra of 1 Ceres, 10 Hygeia, 21 Lutetia, 45 Eugenia, 87 Sylvia, 107 Camilla and NIR spectra of 617 Patroclus and 624 Hektor. The NIR portion of the spectra was acquired with the IRTF on Mauna Kea, Hawaii. The instrument SpeX (Rayner et al., 2003) was utilized in prism mode to obtain measurements covering the wavelength range 0.8–2.5 μm in one exposure. The observing and reduction procedures are well described by Rivkin et al. (2004). *Note*: the NIR spectrum of 624 Hektor is from Emery and Brown (2003). The visible portion of the spectrum was available from SMASS (see Bus and Binzel, 2002a,b). The taxonomic type of each asteroid (Demeo et al., 2009) is indicated directly on the graph.

to those of meteorite analogs. Using data from Ostro et al. (1985), Garvin et al. (1985) and Magri et al. (2001), they found that the surfaces of large main belt asteroids are highly porous over the first meter (40–50% porosity).

### 3.3. Photometric and polarimetric phase effects

Photometric phase effects, such as the opposition effect, the overall phase function, and the so-called amplitude-phase relationship, provide insight into the physical characteristics of the surface, such as surface roughness and porosity. Similarly, polarimetric phase effects, the negative degree of linear polarization in particular, unveil single-particle properties (Muinonen et al., 2002, 2009, 2010).

In the case of the Moon, the strong optical opposition surge (Hapke, 1981; Shkuratov et al., 2011) has been taken as evidence of a high level of porosity within the upper few millimeters of the surface regolith. Estimates of the porosity in the upper few centimeters are consistently around 50% and drop to 40% within 60 cm of the surface (Carrier et al., 1991). The "best estimate" of the in situ porosity (intra- and inter-granular) for the upper 60 cm of the lunar regolith amounts to 46% (Carrier et al., 1991) consistent with the determination by Shepard et al. (2010) for the largest asteroids.

In the case of TNOs, estimations of the opposition effect amplitude and width also seem to indicate a high level of porosity of the surface regolith (Belskaya et al., 2003).

In the case of asteroids, no firm conclusion has been reached yet in terms of surface porosity based on photometric and/or polarimetric phase effects (Muinonen et al., 2002, 2009, 2010; Belskaya et al., 2009, 2010) although the actual measurements seem to favor such conclusion.

In conclusion, the high surface porosities inferred from both radar reflectivities and thermal inertias of large main belt asteroids imply high surface porosities, of the order of 50% within the first meter, and ~90% within the very first millimeters.

## 4. Mechanism at the origin of the surface porosity

Whereas macro-porosity (Marchis et al., 2008a,b; Consolmagno et al., 2008) is a widespread bulk property of most asteroids re-accreted as rubble piles following catastrophic disruption (Asphaug et al., 2002), the presently inferred high-porosity of the regolith is a priori unrelated to the internal structure (and therefore the macro-porosity) of a given asteroid. Instead, it must be related to either forces acting on the regolith grains or possibly cementing agents such as glasses and salts (this latter aspect being described in more detail in K12).

Scheeres et al. (2010) performed a survey of the known relevant forces (electrostatic forces, solar radiation pressure forces, surface contact cohesive – van der Waals – forces) acting on grains and considered how these forces scale relative to each other as a function of grain size. Whereas their analysis remained to a large extent qualitative, it clearly supports the idea that the interplay of these forces may result in a fairly loose porous regolith. They found that the van der Waals cohesive forces generally exceed electrostatic and solar radiation pressure forces in competing with particle weights. Assuming that the van der Waals forces are dominant, then the overall porosity hardly exceeds ~50% although a proper computational model is required to validate this result. A typical regolith structure would be as shown in Fig. 5 (upper right part). Whereas this porosity value is coherent with that derived from radar albedo measurements (see previous section), it would

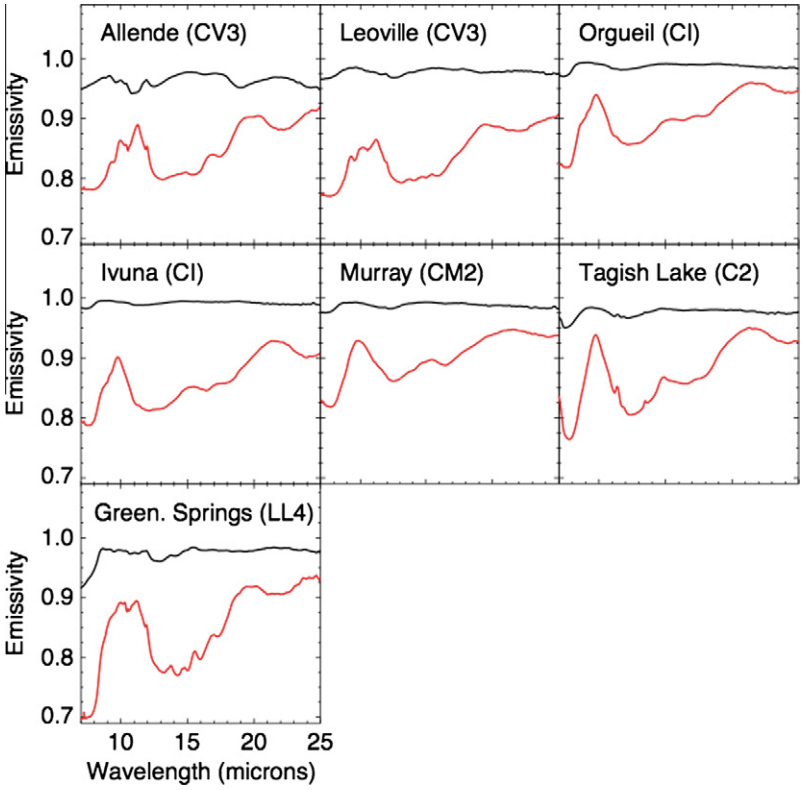


**Fig. 3.** Comparison between the spectra of KBr-diluted (red or lower spectrum) and nonKBr-diluted (black or upper spectrum) meteorites (grain size <30 μm). The spectra were collected at the University of New Mexico (see King et al. for more details). The meteorites and their type are indicated directly on the plot. Biconical reflectance spectra were converted to emissivity using Kirchoff's law ($E = 1–0.03 * R$; with $E$ being emissivity and $R$ being reflectance). [For reasonably small phase angles, under most conditions, biconical reflectance spectra in the mid-IR can be converted to emissivity using Kirchoff's law, with sufficient accuracy for qualitative use in the interpretation of remote sensing data (Korb et al., 1996; Salisbury et al., 1994). (For interpretation of the references to color in this figure legend, the reader is referred to the web version of this article.)

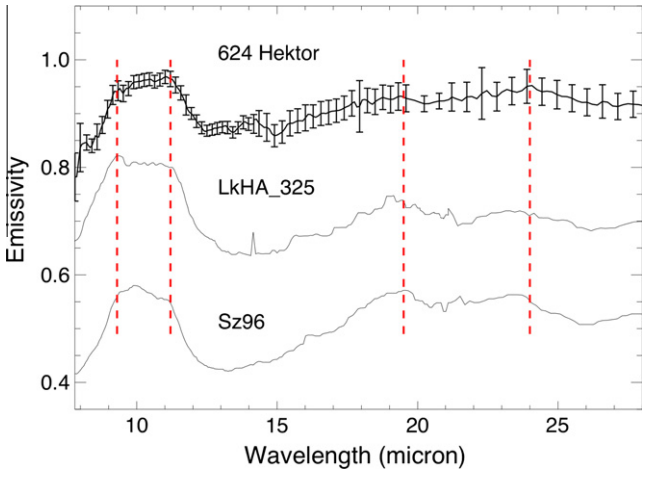


**Fig. 4.** Comparison between the emissivity spectrum of 624 Hektor and the spectra of two protoplanetary disks (LkHA 325 and Sz96, Olofsson et al., 2009). The similarity between the asteroid and disks spectra highlighted by the red dotted lines implies not only similar compositions but also similar scattering properties (in terms of empty space between particles) due to a highly porous surface in the asteroidal case and to particles floating in space in the disk case. In the case of T Tauri disks, the identified features are considered as indicative of the presence of crystalline silicates (e.g. Olofsson et al., 2009, 2010). (For interpretation of the references to color in this figure legend, the reader is referred to the web version of this article.)

probably underestimate the mean porosity of the first millimeter (∼90%) as inferred from both mid-IR spectroscopy and thermal inertia. In this specific case (∼first millimeter), another mechanism may be at work such as dust levitation (see upper left part of Fig. 5), which would increase the overall porosity.

Interestingly, electrostatic transport of charged dust particles has been invoked on a variety of Solar System bodies including the Moon (see Grün et al., 2011 for a review; Zook et al., 1995; Zook and McCoy, 1991; Berg et al., 1974, 1976; Rennilson and Criswell, 1974; McCoy and Criswell, 1973), asteroids (Lee, 1996; Colwell et al., 2005; Hughes et al., 2008), Saturn's rings (Nitter et al., 1998; Goertz, 1989), Saturn's satellite Atlas (Hirata and Miyamoto, 2011), Mercury (Ip, 1986), and comets (Mendis et al., 1981).

Based on observations of lunar dust motion, electrostatic dust levitation and transport has been proposed as a possible explanation for the observed Eros ponds (Cheng et al., 2002; Robinson et al., 2001; Colwell et al., 2005). This explanation was anticipated by Lee (1996) who recognized that levitated charged dust grains over asteroids could be transported to "smooth, flat, and/or perennially shaded areas, or where the particles become physically trapped, e.g., in topographic asperities and/or lows in dynamic height."

Motivated by these observations, considerable research has focused on understanding the electrostatic environment in the sunset/sunrise (terminator) region of the Moon and asteroids. The most recent work by Hartzell and Scheeres (2011) showed that by quantifying the various forces affecting dust particles resting on stationary and seismically active surfaces, the electric field strength required to raise a particle above the surface is at least an order of magnitude larger than the most optimistic current estimates of the electric fields thought to be present in the terminator region, when particle charging is assumed to be governed by

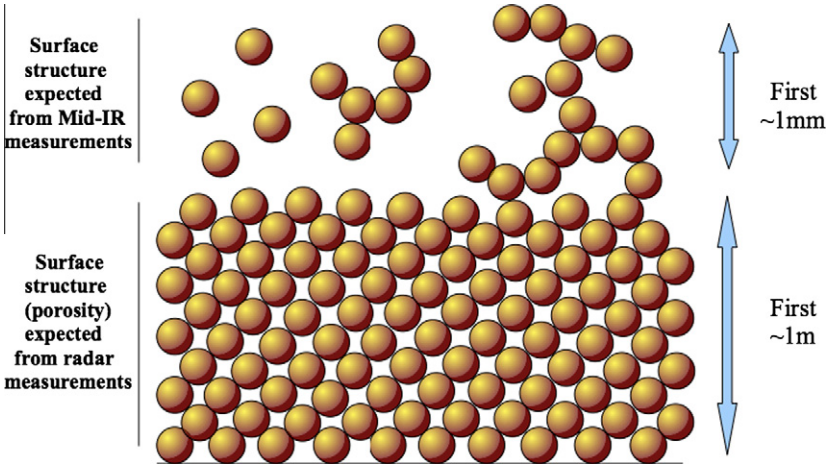


**Fig. 5.** Schematic model of the asteroid surface structure as deduced from both the good correspondance between the KBr-diluted meteorite spectra and the asteroid spectra (for the first millimeter) and the low surface density inferred from radar measurements (for the first meter). The high porosity within the first millimeter may be due to cohesive forces (see model on the upper right-hand side) and/or dust levitation (see model on the upper left-hand side).

Gauss' law. Additional investigations are therefore needed, as the physical mechanism(s) responsible for the high surface porosity of large asteroids remains unknown [see discussion by Hartzell and Scheeres (2011) for ideas].

## 5. Deriving compositional information from mid-IR spectra

In this last section we try to clarify how much compositional information can be retrieved from the mid-IR range. We first focus our analysis on a single object, 624 Hektor, whose spectrum displays the clearest/strongest emissivity features. We next show how this composition helps constraining the origin of Trojan asteroids. Finally, we briefly discuss the necessary/useful wavelength range in the mid-IR for detailed compositional investigation of asteroid surfaces.

### *5.1. Comparison of 624 Hektor's spectrum with KBr-diluted meteorite spectra*

We performed a detailed comparison of Hektor's spectrum with the new mid-IR laboratory measurements of meteorites obtained at the University of New Mexico (King et al., 2011, K12). To search for plausible meteoritic analogs, we used the location of the following diagnostic features: (i) residual reststrahlen features, which occur as reflectance peaks, (ii) absorption bands due to overtone/combination tone bands, which occur as reflectance troughs, and (iii) the Christiansen feature, which also occurs as a trough in reflectance (Salisbury et al., 1991).

The comparison reveals that the closest spectral matches to 624 Hektor are found among ordinary chondrites and carbonaceous chondrites (yet only among CVs, see Fig. 6), that is among olivine-rich meteorites. At first glance, these spectral matches could appear as very surprising since the VNIR spectral properties of ordinary chondrites carbonaceous chondrites (CVs) are at odds with those of Hektor. However, considering that the KBr-diluted samples are very good proxies for small silicate grains being embedded in a highly porous surface layer, the spectral matches make sense. If the grain sizes of the surface particles were very small (<2 μm) as suggested by Emery et al. (2006) in the Trojan case (hence the case of Hektor), then we would not expect to see any absorption band in the VNIR range (as the appearance of such band requires larger grain sizes). The presence of mostly fine-grained olivine particles

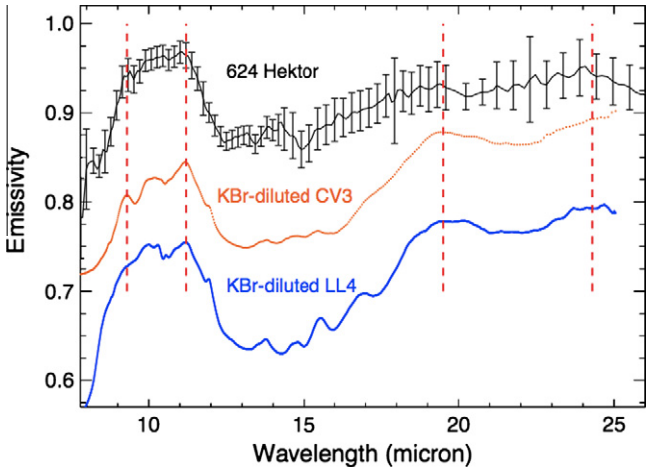


**Fig. 6.** Comparison between the emissivity spectrum of 624 Hektor and the emissivity spectra of the KBr-diluted ordinary chondrite Greenwell Springs (LL4) and the KBr-diluted carbonaceous chondrite Leoville (CV3). The similarities of the spectral features in both the asteroid and meteorite spectra are highlighted by the red dotted lines. As in Fig. 4, the similarity between the asteroid and meteorite spectra implies not only similar compositions (dominated by olivine which we verified with our spectral decomposition model, see Fig. 9 and Table 1) but also similar scattering properties (in terms of empty space between particles) due to a highly porous surface in the asteroidal case. (For interpretation of the references to color in this figure legend, the reader is referred to the web version of this article.)

on these object surfaces would also provide a natural explanation for their red colors, olivine being very sensitive to so-called space weathering processes which tend to redden its VNIR reflectance spectrum (e.g., Vernazza et al., 2009a and references therein). Interestingly and supporting this hypothesis, Emery et al. (2011) successfully modeled the VNIR spectra of red Trojans (note that there are two compositional groups among Trojans – the red and the blue – and Hektor belongs to the red group; see Emery et al., 2011) using amorphous and crystalline silicates (olivine and pyroxene) embedded in a mid-IR transparent matrix as end-members. It thus appears that both their (VNIR range) and our (the mid-IR range) studies predict that the surfaces of red Trojans may be covered by very small silicate grains (mainly olivine) embedded in a highly porous upper surface layer.

### 5.2. Spectral decomposition model applied to 624 Hektor

To further test the idea of the surface of 624 Hektor (hence the surface of red Trojans) being covered by small silicate (olivine, pyroxene) grains, we investigated its surface composition using a spectral decomposition model as commonly implemented by other researchers in the case of cometary and protoplanetary disks spectra (Lisse et al., 2006; Olofsson et al., 2010; Morlok et al., 2010), the physics being roughly the same (i.e., silicate grains being embedded in a transparent medium, see Fig. 4). This is the first time that such technique is applied to an asteroid spectrum.

Hektor's spectrum was modeled as the sum of two contributions originating from two distinct layers as illustrated in Fig. 8:

- The thermal emission of a blackbody at a single temperature ($T_{bb}$) representing the contribution of the 'underlying surface' (i.e., the contribution from the ~1 m layer underlying the 'first' millimeter layer in Fig. 8).
- The thermal emission of the grains forming the 'first' millimeter layer assumed to be at a single temperature ($T_{dust}$) for simplicity.

Concerning the composition of these grains, we used eight different dust species (Table 1), including amorphous and crystalline silicate grains for both olivine and pyroxene species, as well as crystalline silica and amorphous carbon. As grains larger than 10 μm do not show any significant emission features at the expected temperatures on asteroid surfaces, we only considered grain sizes between 0.1 and 10 μm. To quantify the contribution to the total emission of small grains with respect to larger grains, we assumed that the number of grains per bin size obeys a power–law distribution ($dn(\alpha)\ \alpha^p d\alpha$) with power exponent $p$ ($p$ being negative).

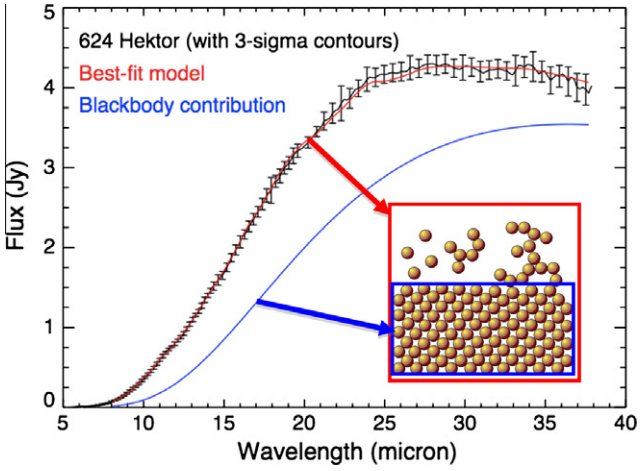


**Fig. 8.** Comparison between Hektor's spectrum (before blackbody removal) and the best-fit model (see Table 1 for the values of the best-fit, the reduced $\chi^2$ for the best-fit is 1.39), which includes the blackbody contribution ($T$ = 140 K; thermal emission from the subsurface). Note that the temperature derived from our model cannot be directly compared with the temperature at the sub solar point calculated by Emery et al. (2006) with the STM as our temperature is a mean value for the entire surface. We also include the schematic model of the asteroid surface structure from Fig. 5 in order to clarify the meaning of both the best fit and the blackbody contribution.

In order to compute the mass absorption coefficients, we relied on the DHS theory combined with optical constants derived from laboratory measurements. The DHS theory, which considers a distribution of hollow spheres (Min et al., 2005), is appropriate

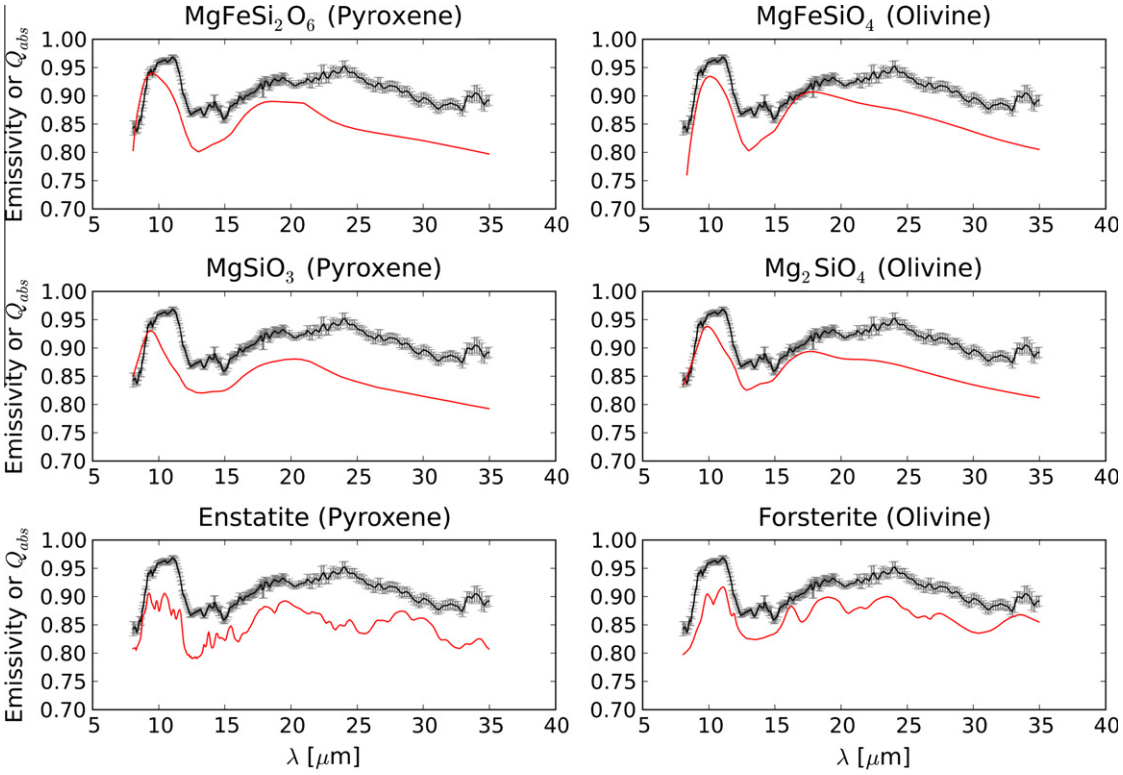


**Fig. 7.** Opacities (in units of $cm^2\ g^{-1}$) used to model Hektor's spectrum are directly compared to the asteroid emissivity spectrum. Left column shows mass absorption coefficients for three members of the pyroxene groups and right column shows the same for three members of the olivine groups. Besides forsterite and enstatite that are crystalline species, all other four phases are amorphous. This qualitative comparison shows that overall, grains from the olivine group provide a better match than grains from the pyroxene group. It is especially true for the crystalline grains, where enstatite features do not match emission features seen in the data, while forsterite provide an interesting comparison.

**Table 1**
Results of the fit of 624 Hektor's spectrum (see Fig. 9).

| Mineral species | Abundance (in mass) | Abundance of the silicates (in mass) |
|---|---|---|
| Silica ($SiO_2$) | 0.00 | – |
| Crystalline olivine | 0.68 | 22.74 |
| Crystalline pyroxene | 0.05 | 1.67 |
| Amorphous olivine [$(MgFe)SiO_4$, $Mg_2SiO_4$] | 2.19 | 73.25 |
| Amorphous pyroxene [$MgSiO_3$, $(MgFe)Si_2O_6$] | 0.07 | 2.34 |
| Amorphous carbon | 97.01 | – |

when attempting to model the emissivity of particles floating in space. Accordingly, it has been employed by other researchers to model the spectra of protoplanetary disks (e.g., Olofsson et al., 2010). We used filling factors of $f_{max} = 0.7$ for amorphous grains (Min et al., 2007) and $f_{max} = 1.0$ for enstatite crystalline grains. Concerning forsterite and silica grains, we utilized the laboratory data acquired with the aerosol technique (e.g., Tamanai et al., 2009) as this approach provides measurements that are less subject to environmental effects, such as electromagnetic polarization of the embedding medium (KBr, cesium iodine, polyethylene) when using them for the pellet technique.

Finally, we computed for each dust specie an averaged opacity (emission efficiency of the particle due to its composition), weighted by the number of grains per bin size according to the size distribution function. All resulting averaged opacities were then multiplied by a Planck function at temperature $T_{dust}$. Finally, the best fit to the spectrum of Hektor was obtained as a linear combination of these average opacities. The free parameters (the relative contribution of the eight dust species, $T_{dust}$, $T_{bb}$, $p$) were determined using a Levenberg–Marquardt minimization algorithm.

The best-fit solution characterized by a reduced $\chi^2$ of 1.39 corresponds to $T_{bb} = 140$ K, $T_{dust} = 150$ K and relative contributions of the different dust species listed in Table 1. The model spectrum is shown in Figs. 8 and 9 and the mass absorption coefficients of the different dust species are directly compared to Hektor's emissivity spectrum in Fig. 7.

Whereas the match is satisfactory, one should keep in mind the very low contrast of the emission features in the asteroid data so that the result of the fitting procedure must be carefully interpreted. Specifically, we do not claim to determine the dust composition at a level of a few percent; yet, we can distinguish compositional trends that seem quite robust. It first appears that both amorphous and crystalline grains are present on Hektor's surface (75% versus 25%, see Table 1). Second, it seems that olivine are much more abundant than pyroxene grains (96% versus 4%,). These trends are supported by both the presence of emission features in Hektor's emissivity spectrum, especially around 24 μm and 28 μm, which are consistent with those of crystalline olivine grains (Fig. 7), and also by our analysis presented in the previous section.

### 5.3. Origin of the red Trojans

The presence of both amorphous and crystalline silicates on Hektor's surface indicates that its bulk material has not been heated above ~1000 K for any significant length of time since its assemblage. If its surface material had experienced such heating, then the amorphous components would have annealed and crystallized (Roskosz et al., 2011). An analogy may be made with slightly-metamorphosed carbonaceous chondrites, which contain abundant high-temperature components (e.g., feldspathic glass, crystalline pyroxene and olivine, presolar diamond and SiC grains) intimately mixed with low-temperature components (e.g., organic compounds, hydrous phases). What we know of cometary materials (from infrared observations and analysis of samples from the Stardust mission) also shows that comets contain high-temperature components (including glasses) intimately mixed with slightly metamorphosed material. These phase assemblages indicate that the comets and carbonaceous chondrite parent objects (or at least the parts of them that we can see/sample) have not undergone bulk heating over significant timescales.

An explanation to the simultaneous presence of low-temperature (amorphous) and high-temperature (crystalline) solar nebular condensates on the surface of Hektor is that crystalline silicates were thermally processed prior to accretion (which is also the case for comets) and have been subsequently mixed from the hot inner-solar nebula into the Trojan forming zone perhaps by turbulent diffusion (Wehrstedt and Gail, 2003; Wooden et al., 2007) or by large-scale radial flows (Keller and Gail, 2004; Ciesla, 2007). The presence of crystalline silicates at large distances in both our Solar System (e.g., in comets, see Lisse et al., 2006; Brownlee et al., 2006) and in disks around other stars (Olofsson et al., 2010) suggests that the presence of such grains at large distances is a fundamental consequence of protoplanetary disk evolution.

All in all, the composition of the grains at the surface of Hektor inferred from this work is close to that composition of cometary grains (Brunetto et al., 2011), which may imply a similar – yet not necessarily identical – formation location for both comets and red Trojans. Emery et al. (2006) also noticed the striking similarity between the mid-IR spectra of these two populations.

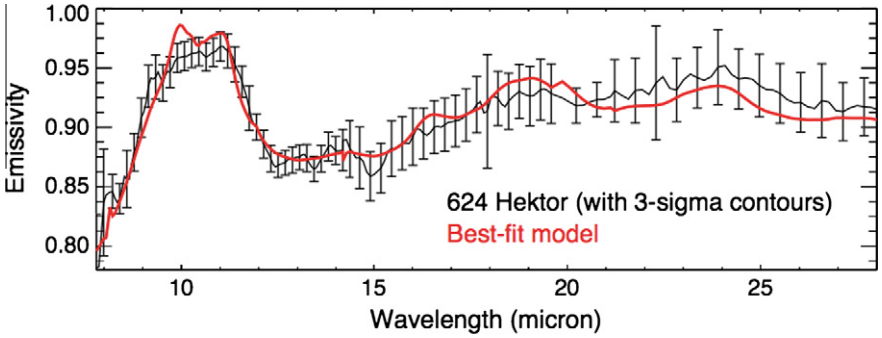


**Fig. 9.** Comparison between Hektor's spectrum and the best-fit model (see Table 1 for the values of the best-fit). Based on the best-fit model, it appears that both amorphous and crystalline grains are present on Hektor's surface. Second, it seems that olivine grains are more abundant than pyroxene grains (see Table 1).

Importantly, both the compelling match between Hektor's spectrum and the spectra of KBr-diluted ordinary chondrites and KBr-diluted carbonaceous chondrites (yet only among CVs) on the one hand, and the composition of Hektor derived from the spectral decomposition model on the other hand indicate that its composition (and thus the surface composition of red Trojans) is dominated by olivine. Assuming that Hektor and the red Trojans in general formed in the same region as comets [as suggested by Emery et al. (2011) and our own result], this work provides an important constraint on the primordial composition of the dust present in the outer part (>10 AU) of the Solar System's protoplanetary disk. Putting this result in the global picture of many different types of circumstellar disks (Olofsson et al., 2009, 2010) may help deciphering the early evolution of our own protoplanetary disk.

### 5.4. Which is the mid-IR wavelength range that carries the most relevant compositional information?

Although it has not been the main focus of the paper, this study has shown that the 7.5–13 μm range alone is not always sufficient for constraining the surface composition of an asteroid; on the positive side, this 'limited' wavelength range gives important constraints on the surface structure (low/high surface porosity determined by the presence/absence of the 10-μm emissivity band).

Although it covers well the 10-μm emissivity band of all observed asteroids, this range does not include additional features that play an important role when deciphering the composition of an asteroid as already noticed by Lim et al. (2011) in the case of 956 Elisa and by Vernazza et al. (2011) in the case of 21 Lutetia. Specifically, one would hardly make the distinction between for instance 21 Lutetia and 624 Hektor based on spectral information within this range, confirming its sometimes-limited diagnostic capabilities (Vernazza et al., 2010). Note the paramount importance of sample preparation (KBr-diluted or nonKBr-diluted) for the correct interpretation of asteroid data in the mid-IR range as demonstrated in the present work.

Based on the specific cases of both Lutetia and Hektor, the complementing spectral range 13–25 μm unveils additional emission bands (e.g., ~19 and ~24 μm in the case of Hektor), which help deciphering their surface composition. Altogether, the mid-IR domain (7–25 μm) reveals itself as a powerful tool for constraining the surface composition of asteroids with porous surfaces and therefore their origin (the region of terrestrial planets in the case of Lutetia and the formation region of comets in the case of Hektor).

Similarly, in the case of protoplanetary disks, it is also found that extending the wavelength coverage to ~30 μm allows constraining the presence/abundance of crystalline material more rigorously than with the ~7–13 μm emission spectrum alone. This is because some of the crystalline species exhibit several spectral signatures from 13 to 30 μm.

## 6. Conclusions

Emission features in the mid-IR domain (7–25 μm) are quite ubiquitous among large asteroids and therefore offer the potential to uncover their surface composition. However, when comparing these spectra with the actual laboratory spectra of both minerals and meteorites, they do not necessarily match. Here, and in a companion paper by King et al. (in preparation, 2012), we show that by modifying the sample preparation – typically by suspending meteorite and/or mineral powder (<30 μm) in IR-transparent KBr (potassium bromide) powder – we are able to reproduce the spectral behavior of those main-belt asteroids with emissivity features. This resulting good match between KBr-diluted meteorite spectra and asteroid spectra suggests an important surface porosity (>90%) for the first millimeter for our asteroid sample. It therefore appears that mid-IR emission spectra of asteroids do not only carry information about their surface composition but they can also help us constraining their surface structure (under-dense versus compact surface structure), as suggested by Emery et al. (2006) in the case of the Jupiter Trojans. The large surface porosity inferred from the mid-IR spectra of certain asteroids is also implied by two other independent measurements, namely their thermal inertia and their radar albedo.

According to our result, one should use measurements of KBr-diluted minerals and meteorites in order to interpret the surface composition of asteroids with porous surfaces. Since such measurements are still rare, many more laboratory measurements of KBr-diluted minerals and meteorites need to be performed. Conversely, the correspondence between KBr-diluted meteorite spectra and asteroid spectra is not expected for objects with a low surface porosity (high thermal inertia). In those cases, one would expect the usual meteorite spectra (available in the RELAB and ASTER databases) to provide the relevant comparison. These non-diluted meteorite spectra are suitable for comparison with high thermal inertia asteroids in agreement with the flat spectra of 25143 Itokawa (Vernazza et al., 2010) and of 1999 RQ36 (Emery et al., 2010).

Our detailed compositional analysis of the spectrum of Hektor has allowed us to ascertain its composition and place its origin in the formation regions of comets.

Finally, future investigations should focus on finding the mechanism responsible for creating such high surface porosity.

## Acknowledgments

The research leading to these results has received funding from the European Community's Seventh Framework Programme (/FP7/2007-2013/) under Grant Agreement No. 229517. Franck Marchis is supported by NASA Grant NNX11AD62G.

Part of the data utilized in this publication were obtained and made available by The MIT-UH-IRTF Joint Campaign for NEO Reconnaissance. The IRTF is operated by the University of Hawaii under Cooperative Agreement No. NCC 5-538 with the National Aeronautics and Space Administration, Office of Space Science, Planetary Astronomy Program. The MIT component of this work is supported by NASA Grant 09-NEOO009-0001, and previously by the National Science Foundation under Grant No. 0506716.

## References

Asphaug, E., Ryan, E.V., Zuber, M.T., 2002. Asteroid interiors. In: Bottke, W.F., Jr., Cellino, A., Paolicchi, P., Binzel, R.P. (Eds.), Asteroids III. University of Arizona, Tucson, pp. 463–484.

Barucci, M.A. et al., 2002. 10 Hygiea: ISO infrared observations. Astron. Astrophys. 156, 202–210.

Barucci, M.A. et al., 2008. Asteroids 2867 Steins and 21 Lutetia: Surface composition from far infrared observations with the Spitzer space telescope. Astron. Astrophys. 477, 665–670.

Belskaya, I.N., Barucci, A.M., Shkuratov, Y.G., 2003. Opposition effect of Kuiper belt objects: Preliminary estimations. Earth, Moon, Planets 92, 201–206.

Belskaya, I.N., Levasseur-Regourd, A.-C., Cellino, A., Efimov, Y.S., Shakhovskoy, N.M., Hadamcik, E., Bendjoya, P., 2009. Polarimetry of main belt asteroids: Wavelength dependence. Icarus 199, 97–105.

Belskaya, I.N. et al., 2010. Puzzling Asteroid 21 Lutetia: Our knowledge prior to the Rosetta fly-by. Astron. Astrophys. 515, id.A29.

Berg, O.E., Richardson, F.F., Rhee, J.W., Auer, S., 1974. Preliminary results of a cosmic dust experiment on the Moon. Geophys. Res. Lett. 1, 289–290.

Berg, O.E., Wolf, H., Rhee, J., 1976. Lunar soil movement registered by the Apollo 17 cosmic dust experiment. In: Elsässer, H., Fechtig, H. (Eds.), Interplanetary Dust and Zodiacal Light. Springer-Verlag, Heidelberg, pp. 233–237.

Binzel, R.P., Xu, S., 1993. Chips off of Asteroid 4 Vesta: Evidence for the parent body of basaltic achondrite meteorites. Science 260, 186–191.

Binzel, R.P., Rivkin, A.S., Bus, S.J., Sunshine, J.M., Burbine, T.H., 2001. MUSES-C target Asteroid (25143) 1998 SF36: A reddened ordinary chondrite. Meteorit. Planet. Sci. 36, 1167–1172.
Binzel, R.P., Rivkin, A.S., Thomas, C.A., Vernazza, P., Burbine, T.H., DeMeo, F.E., Bus, S.J., Tokunaga, A.T., Birlan, M., 2009. Spectral properties and composition of potentially hazardous Asteroid (99942) Apophis. Icarus 200, 480–485.
Binzel, R.P. et al., 2010. Earth encounters as the origin of fresh surfaces on near-Earth asteroids. Nature 463, 331–334.
Bottke, W.F., Nesvorny, D., Grimm, R.E., Morbidelli, A., O'Brien, D.P., 2006. Iron meteorites as remnants of planetesimals formed in the terrestrial planet region. Nature 439, 821–824.
Brownlee, D. et al., 2006. Comet 81P/Wild 2 under a microscope. Science 314, 1711–1716.
Brunetto, R., Borg, J., Dartois, E., Rietmeijer, F.J.M., Grossemy, F., Sandt, C., Le Sergeant D'Hendecourt, L., Rotundi, A., Dumas, P., Djouadi, Z., Jamme, F., 2011. Mid-IR, far-IR, Raman micro-spectroscopy, and FESEM-EDX study of IDP L2021C5: Clues to its origin. Icarus 212, 896–910.
Bus, S.J., Binzel, R.P., 2002a. Phase II of the Small Main-belt Asteroid Spectroscopic Survey: The observations. Icarus 158, 106–145.
Bus, S.J., Binzel, R.P., 2002b. Phase II of the Small Main-belt Asteroid Spectroscopic Survey: A feature-based taxonomy. Icarus 158, 146–177.
Carrier III, W.D., Olhoeft, G.R., Mendell, W., 1991. Physical properties of the lunar surface. In: Heiken, G.W., Vaniman, D.T., French, B.M. (Eds.), Lunar Sourcebook: A User's Guide to the Moon. Cambridge University Press, NY, pp. 475–594.
Cheng, A.F., Izenberg, N., Chapman, C.R., Zuber, M.T., 2002. Ponded de- posits on Asteroid 433 Eros. Meteorit. Planet. Sci. 37, 1095–1105.
Ciesla, Fred J., 2007. Outward transport of high-temperature materials around the midplane of the solar nebula. Science 318, 613–615.
Clark, B.E. et al., 2010. Spectroscopy of B-type asteroids: Subgroups and meteorite analogs. J. Geophys. Res. 115, E06005.
Cohen, M., Witteborn, F.C., Roush, T., Bregman, J., Wooden, D., 1998. Spectral irradiance calibration in the infrared. VIII. 5–14 Mm spectroscopy of the asteroids Ceres, Vesta, and Pallas. Astron. J. 115, 1671–1679.
Colwell, J.E., Gulbis, A.A.S., Horányi, M., Robertson, S., 2005. Dust transport in photoelectron layers and the formation of dust ponds on Eros. Icarus 175, 159–169.
Consolmagno, G., Britt, D., Macke, R., 2008. The significance of meteorite density and porosity. Chem. Erde 68, 1–29.
Consolmagno, G., Opeil, C.P., Britt, D.T., 2010. Thermal Conductivities of Two Basaltic Achondrite Meteorites. DPS, vol. 42, p. 970.
Crovisier, J. et al., 1997. The spectrum of comet Hale-Bopp (C/1995 O1) observed with the Infrared Space Observatory at 2.9 astronomical units from the Sun. Science 275, 1904–1907.
Cruikshank, D., Hartmann, W.K., 1984. The meteorite–asteroid connection: Two olivine-rich asteroids. Science 223, 281–283.
de León, J., Licandro, J., Serra-Ricart, M., Pinilla-Alonso, N., Campins, H., 2010. Observations, compositional, and physical characterization of near-Earth and Mars-crosser asteroids from a spectroscopic survey. Astron. Astrophys. 517, id.A23.
de León, J., Pinilla-Alonso, N., Campins, H., Licandro, J., Marzo, G.A., 2012. Near-infrared spectroscopic survey of B-type asteroids: Compositional analysis. Icarus 218, 196–206.
Delbo', M., Tanga, P., 2009. Thermal inertia of main belt asteroids smaller than 100 km from IRAS data. Planet. Space Sci. 57, 259–265.
Delbo', M., Dell'Oro, A., Harris, A.W., Mottola, S., Mueller, M., 2007. Thermal inertia of near-Earth asteroids and implications for the magnitude of the Yarkovsky effect. Icarus 190, 236–249.
Demeo, F.E., Binzel, R.P., Slivan, S., Bus, S.J., 2009. An extension of the bus asteroid taxonomy into the near-infrared. Icarus 202, 160–180.
Dotto, E., Barucci, M.A., Brucato, J.R., Müller, T.G., Carvano, J., 2004. 308 Polyxo: ISO-SWS spectrum up to 26 μm. Astron. Astrophys. 427, 1081–1084.
Duffard, R., Lazzaro, D., Licandro, J., de Sanctis, M.C., Capria, M.T., Carvano, J.M., 2004. Mineralogical characterization of some basaltic asteroids in the neighborhood of (4) Vesta: First results. Icarus 171, 120–132.
Emery, J.P., Brown, R.H., 2003. Constraints on the surface composition of Trojan asteroids from near infrared (0.8–4.0 μm) spectroscopy. Icarus 164, 104–121.
Emery, J.P., Cruikshank, D.P., van Cleve, J., 2006. Thermal emission spectroscopy (5.238 μm) of three Trojan asteroids with the Spitzer Space Telescope: Detection of fine-grained silicates. Icarus 182, 496–512.
Emery, J.P. et al., 2010. Thermophysical Characterization of Potential Spacecraft Target (101955) 1999 RQ36. Lunar Planet. Sci.1533.
Emery, J.P., Burr, D.M., Cruikshank, D.P., 2011. Near-infrared spectroscopy of Trojan asteroids: Evidence for two compositional groups. Astron. J. 141, id.25.
Gaffey, M.J., 1997. Surface lithologic heterogeneity of Asteroid 4 Vesta. Icarus 127, 130–157.
Gaffey, M.J. et al., 1993. Mineralogical variations within the S-type asteroid class. Icarus 106, 573–602.
Garvin, J.B., Head, J.W., Pettengill, G.H., Zisk, S.H., 1985. Venus global radar reflectivity and correlations with elevation. J. Geophys. Res. 90, 6859–6871.
Goertz, C.K., 1989. Dusty plasmas in the Solar System. Rev. Geophys. 27 (2), 271–292.
Gomes, R., Levison, H.F., Tsiganis, K., Morbidelli, A., 2005. Origin of the cataclysmic Late Heavy Bombardment period of the terrestrial planets. Nature 435, 466–469.
Grün, E., Horanyi, M., Sternovsky, Z., 2011. The lunar dust environment. Planet. Space Sci. 59, 1672–1680.
Hapke, B., 1981. Bidirectional reflectance spectroscopy. 1. Theory. J. Geophys. Res. 86, 3039–3054.
Hartzell, C.M., Scheeres, D.J., 2011. The role of cohesive forces in particle launching on the Moon and asteroids. Planet. Space Sci. 59, 1758–1768.
Hirata, N.H., Miyamoto, H.M., 2011. Unusual Smoothness of the Surface of a Saturnian Icy Satellite, Atlas. Lunar Planet. Sci. 1608, 1716.
Hiroi, T., Zolensky, M.E., Pieters, C.M., 2001. The Tagish Lake meteorite: A possible sample from a D-type asteroid. Science 293, 2234–2236.
Hughes, A.L.H., Colwell, J.E., Dewolfe, A.W., 2008. Electrostatic dust transport on Eros: 3-D simulations of pond formation. Icarus 195, 630–648.
Ip, W.H., 1986. Electrostatic charging and dust transport at Mercury's surface. Geophys. Res. Lett. 13, 1133–1136.
Izawa, M.R.M., King, P.L., Flemming, R.L., Peterson, R.C., McCausland, P.J.A., 2010. Mineralogical and spectroscopic investigation of enstatite chondrites by X-ray diffraction and infrared reflectance spectroscopy. J. Geophys. Res. 115, E07008.
Keller, Ch., Gail, H.-P., 2004. Radial mixing in protoplanetary accretion disks. VI. Mixing by large-scale radial flows. Astron. Astrophys. 415, 1177–1185.
King, P.L., Izawa, M.R.M., Vernazza, P., McCutcheon, W.A., Berger, J.A., Dunn, T. 2011. Salt—A Critical Material to Consider when Exploring the Solar System. Lunar Planet. Sci. 1608.
Korb, A.R., Dybwad, P., Wadsworth, W., Salisbury, J.W., 1996. Portable FTIR spectrometer for field measurements of radiance and emissivity. Appl. Opt. 35, 1679–1692.
Lazzaro, D. et al., 2000. Discovery of a basaltic asteroid in the outer main belt. Science 288, 2033–2035.
Lee, P., 1996. Dust levitation on asteroids. Icarus 124, 181–194.
Levison, H.F., Bottke, W.F., Gounelle, M., Morbidelli, A., Nesvorny, D., Tsiganis, K., 2009. Contamination of the asteroid belt by primordial trans-neptunian objects. Nature 460, 364–366.
Licandro, J. et al., 2011. (65) Cybele: Detection of small silicate grains, water–ice, and organics. Astron. Astrophys. 525, id.A34.
Licandro, J. et al., 2012. 5–14 μm Spitzer spectra of Themis family asteroids. Astron. Astrophys. 537, id.A73.
Lim, L.F., Emery, J.P., Moskovitz, N.A., 2011. Mineralogy and thermal properties of V-type Asteroid 956 Elisa: Evidence for diagenetic material from the Spitzer IRS (5–35 μm) spectrum. Icarus 213, 510–523.
Lisse, C.M. et al., 2006. Spitzer Spectral Observations of the Deep Impact Ejecta. Science 313, 635–640.
Magri, C., Consolmagno, G.J., Ostro, S.J., Benner, L.A.M., Beeney, B.R., 2001. Radar constraints on asteroid regolith properties using 433 Eros as ground truth. Meteorit. Planet. Sci. 36, 1697–1709.
Marchis, F., Descamps, P., Berthier, J., Hestroffer, D., Vachier, F., Baek, M., Harris, A.W., Nesvorný, D., 2008a. Main belt binary asteroidal systems with eccentric mutual orbits. Icarus 195 (1), 295–316.
Marchis, F., Descamps, P., Baek, M., Harris, A., Kaasalainen, M., Berthier, J., Hestroffer, D., Vachier, F., 2008b. Main belt binary asteroidal systems with circular mutual orbits. Icarus 196 (1), 97–118.
Marchis et al., submitted for publication. Multiple asteroid systems: Dimensions and thermal properties from Spitzer Space Telescope and ground-based observations. Icarus..
McCord, T.B., Adams, J.B., Johnson, T.V., 1970. Asteroid Vesta: Spectral reflectivity and compositional implications. Science 168, 1445–1447.
McCoy, J.E., Criswell, D.R., 1973. Evidence for a high altitude distribution of lunar dust. Proc. Lunar Sci. Conf. 5, 496–497.
Mendis, D.A., Hill, J.R., Houpis, H.L.F., Whipple Jr., E.C., 1981. On the electrostatic charging of the cometary nucleus. Astrophys. J. 249, 787–797.
Min, M., Hovenier, J.W., de Koter, A., 2005. Modeling optical properties of cosmic dust grains using a distribution of hollow spheres. Astron. Astrophys. 432, 909–920.
Min, M., Waters, L.B.F.M., de Koter, A., Hovenier, J.W., Keller, L.P., Markwick-Kemper, F., 2007. The shape and composition of interstellar silicate grains. Astron. Astrophys. 462, 667–676.
Morbidelli, A., Levison, H.F., Tsiganis, K., Gomes, R., 2005. Chaotic capture of Jupiter's Trojan asteroids in the early Solar System. Nature 435, 462–465.
Morlok, A., Koike, C., Tominoka, N., Mann, I., Tomeoka, K., 2010. Mid-IR spectra of the shocked Murchison CM chondrite: Comparison with astronomical observations of dust in debris disks. Icarus 207, 45–53.
Moskovitz, N.A., Jedicke, R., Gaidos, E., Willman, M., Nesvorný, D., Fevig, R., Ivezić, Ž., 2008. The distribution of basaltic asteroids in the main belt. Icarus 198, 77–90.
Mueller, M., Marchis, F., Emery, J.P., Harris, A.W., Mottola, S., Hestroffer, D., Berthier, J., di Martino, M., 2010. Eclipsing binary Trojan asteroid Patroclus: Thermal inertia from Spitzer observations. Icarus 205, 505–515.
Muinonen, K., Piironen, J., Shkuratov, Yu.G., Ovcharenko, A., Clark, B.E., 2002. Asteroid photometric and polarimetric phase effects. In: Bottke, W.F., Jr., Cellino, A., Paolicchi, P., Binzel, R.P. (Eds.), Asteroids III. University of Arizona Press, Tucson, pp. 23–138.
Muinonen, K. et al., 2009. Asteroid photometric and polarimetric phase curves: Joint linear-exponential modeling. Meteorit. Planet. Sci. 44, 1937–1946.
Muinonen, K., Tyynelä, J., Zubko, E., Videen, G., 2010. Scattering parameterization for interpreting asteroid polarimetric and photometric phase effects. Earth, Planets Space 62, 47–52.
Nitter, T., Havnes, O., Melandsø, F., 1998. Levitation and dynamics of charged dust in the photoelectron sheath above surfaces in space. J. Geophys. Res. 103, 6605–6620.
Olofsson, J. et al., 2009. C2D Spitzer-IRS spectra of disks around T Tauri stars. IV. Crystalline silicates. Astron. Astrophys. 507, 327–345.

Olofsson, J. et al., 2010. C2D Spitzer-IRS spectra of disks around T Tauri stars. V. Spectral decomposition. Astron. Astrophys. 520, id.A39.
Opeil, C.P., Consolmagno, G.J., Britt, D.T., 2010. The thermal conductivity of meteorites: New measurements and analysis. Icarus 208, 449–454.
Ostro, S.J., Campbell, D.B., Shapiro, I.I., 1985. Mainbelt asteroids: Dual polarization radar observations. Science 229, 442–446.
Rayner, J.T. et al., 2003. A medium-resolution 0.8–5.5 μm spectrograph and imager for the NASA Infrared Telescope Facility. PASP 115, 362–382.
Reddy, V., Emery, J.P., Gaffey, M.J., Bottke, W.F., Cramer, A., Kelley, M.S., 2009. Composition of 298 Baptistina: Implications for the K/T impactor link. Meteorit. Planet. Sci. 44, 1917–1927.
Reddy, V., Gaffey, M.J., Kelley, M.S., Nathues, A., Li, J., Yarbrough, R., 2010. Compositional heterogeneity of Asteroid 4 Vesta's southern hemisphere: Implications for the Dawn mission. Icarus 210, 693–706.
Reddy, V., Nathues, A., Gaffey, M.J., Schaeff, S., 2011. Mineralogical characterization of potential targets for the ASTEX mission scenario. Planet. Space Sci. 59, 772–778.
Rennilson, J.J., Criswell, D.R., 1974. Surveyor observations of lunar horizon glow. The Moon 10, 121–142.
Rivkin, A.S., Binzel, R.P., Sunshine, J., Bus, S.J., Burbine, T.H., Saxena, A., 2004. Infrared spectroscopic observations of 69230 Hermes (1937 UB) and (19356) 1997GH3: Possible unweathered endmembers among ordinary chondrite analogs. Icarus 172, 408–414.
Robinson, M.S., Thomas, P.C., Veverka, J., Murchie, S., Carcich, B., 2001. The nature of ponded deposits on Eros. Nature 413, 396–400.
Roig, F., Nesvorný, D., Gil-Hutton, R., Lazzaro, D., 2008. V-type asteroids in the middle main belt. Icarus 194, 125–136.
Roskosz, M., Gillot, J., Capet, F., Roussel, P., Leroux, H., 2011. A sharp change in the mineralogy of annealed protoplanetary dust at the glass transition temperature. Astron. Astrophys. 529, id.A111.
Salisbury, J.W., D'Aria, D.M., Jarosewich, E., 1991. Midinfrared (2.5–13.5 μm) reflectance spectra of powdered stony meteorites. Icarus 92, 280–297.
Salisbury, J.W., Wald, A., D'Aria, D.M., 1994. Thermal-infrared remote sensing and Kirchhoff's law 1. Laboratory measurements. J. Geophys. Res. 99, 11897–11911.
Scheeres, D.J., Hartzell, C.M., Sánchez, P., Swift, M., 2010. Scaling forces to asteroid surfaces: The role of cohesion. Icarus 210, 968–984.
Shepard, M.K., Clark, B.E., Ockert-Bell, M., Nolan, M.C., Howell, E.S., Magri, C., Giorgini, J.D., Benner, L.A.M., Ostro, S.J., Harris, A.W., 3 coauthors, 2010. A radar survey of M- and X-class asteroids II. Summary and synthesis. Icarus 208, 221–237.
Shkuratov, Y., Kaydash, V., Korokhin, V., Velikodsky, Y., Opanasenko, N., Videen, G., 2011. Optical measurements of the Moon as a tool to study its surface. Planet. Space Sci. 59, 1326–1371.
Sunshine, J.M., Bus, S.J., McCoy, T.J., Burbine, T.H., Corrigan, C.M., Binzel, R.P., 2004. High-calcium pyroxene as an indicator of igneous differentiation in asteroids and meteorites. Meteorit. Planet. Sci. 39, 1343–1357.
Sunshine, J.M., Bus, S.J., Corrigan, C.M., McCoy, T.J., Burbine, T.H., 2007. Olivine-dominated asteroids and meteorites: Distinguishing nebular and igneous histories. Meteorit. Planet. Sci. 42, 155–170.
Tamanai, A., Mutschke, H., Blum, J., Posch, Th., Koike, C., Ferguson, J.W., 2009. Morphological effects on IR band profiles. Experimental spectroscopic analysis with application to observed spectra of oxygen-rich AGB stars. Astron. Astrophys. 501, 251–267.
Tsiganis, K., Gomes, R., Morbidelli, A., Levison, H.F., 2005. Origin of the orbital architecture of the giant planets of the Solar System. Nature 435, 459–461.
Vernazza, P. et al., 2005. Analysis of near-IR spectra of 1 Ceres and 4 Vesta, targets of the Dawn mission. Astron. Astrophys. 436, 1113–1121.
Vernazza, P. et al., 2008. Compositional differences between meteorites and near-Earth asteroids. Nature 454, 858–860.
Vernazza, P., Brunetto, R., Binzel, R.P., Perron, C., Fulvio, D., Strazzulla, G., Fulchignoni, M., 2009a. Plausible parent bodies for enstatite chondrites and mesosiderites: Implications for Lutetia's fly-by. Icarus 202, 477–486.
Vernazza, P., Binzel, R.P., Rossi, A., Fulchignoni, M., Birlan, M., 2009b. Solar wind as the origin of rapid reddening of asteroid surfaces. Nature 458, 993–995.
Vernazza, P., Carry, B., Emery, J., Hora, J.L., Cruikshank, D., Binzel, R.P., Jackson, J., Helbert, J., Maturilli, A., 2010. Mid-IR spectral variability for compositionally similar asteroids: Implications for asteroid particle size distributions. Icarus 207, 800–809.
Vernazza, P., Lamy, P., Groussin, O., Hiroi, T., Jorda, L., King, P.L., Izawa, M.R.M., Marchis, F., Birlan, M., Brunetto, R., 2011. Asteroid (21) Lutetia as a remnant of Earth's precursor planetesimals. Icarus 216, 650–659.
Walsh, K.J., Morbidelli, A., Raymond, S.N., O'Brien, D.P., Mandell, A.M., 2011. A low mass for Mars from Jupiter's early gas-driven migration. Nature 475, 206–209.
Wehrstedt, M., Gail, H.-P., 2003. Radial mixing in protoplanetary accretion disks. V. Models with different element mixtures. Astron. Astrophys. 410, 917–935.
Wooden, D., Desch, S., Harker, D., Gail, H.-P., Keller, L., 2007. Comet grains and implications for heating and radial mixing in the protoplanetary disk. In: Reipurth, V.B., Jewitt, D., Keil, K. (Eds.), Protostars and Planets. University of Arizona Press, Tucson, pp. 815–833.
Ziffer, J., Campins, H., Licandro, J., Walker, M.E., Fernandez, Y., Clark, B.E., Mothe-Diniz, T., Howell, E., Deshpande, R., 2011. Near-infrared spectroscopy of primitive asteroid families. Icarus 213, 538–546.
Zimbelman, J.R., 1986. The role of porosity in thermal inertia variations on basaltic lavas. Icarus 68, 366–369.
Zook, H.A., McCoy, J.E., 1991. Large-scale lunar horizon glow and a high altitude lunar dust exosphere. Geophys. Res. Lett. 18, 2117–2120.
Zook, H.A., Potter, A.E., Cooper, B.L., 1995. The lunar dust exosphere and Clementine lunar horizon glow. Lunar Planet. Sci. 26, 1577–1578.